*J. Fluid Mech.* (1996), *vol.* 313, *pp.* 209–222



# The structure of the vortices in freely decaying two-dimensional turbulence

By JAVIER JIMÉNEZ[1], H. K. MOFFATT[2] AND CARLOS VASCO[1]

[1]School of Aeronautics, Pl. Cardenal Cisneros 3, 28040 Madrid, Spain

[2]Department of Applied Mathematics and Theoretical Physics, University of Cambridge Silver Street, Cambridge CB3 9EW, UK

(Received 23 June 1995)

The structure of a viscous two-dimensional vortex core in a imposed weak strain is analysed, in the same spirit as a similar analysis of strained columnar vortices (Moffatt, Kida & Ohkitani 1994). The analysis is recast in terms of a coordinate deformation, ensuring the uniform validity of the perturbation expansion up to the neighbourhood of a dividing streamline, beyond which it is not expected to work, and from where the exponentially weak vorticity is expected to be stripped to infinity. The orientation and ellipticity of the vorticity distribution of the cores is compared with the results of a numerical experiment in two-dimensional turbulence, and shown to agree. This is interpreted both as a confirmation of the theory and as an indication that the vortices of two-dimensional turbulence are sufficiently long-lived to be controlled by viscous diffusion, even at the relatively large Reynolds numbers of our simulation.

## 1. Introduction

The structure of equilibrium stretched vortices in a weak triaxial strain was analysed by Moffatt, Kida & Ohkitani (1994, hereafter referred to as MKO94). It was found that, in the limit of high circulation Reynolds number, $Re_\Gamma = \Gamma/\nu$, an equilibrium configuration exists which is controlled by viscosity. A similar conclusion was reached by Ting & Tung (1965) for two-dimensional viscous vortices in a potential driving flow, when the characteristic vorticity of the cores was much larger than the applied strain. We shall address in this paper the case of a two-dimensional vortex in a weak constant strain field, in the spirit of the asymptotic expansion in MKO94, and we shall compare the predictions of the analysis to the vortices contained in a catalogue obtained from a numerical simulation of two-dimensional turbulence. Although in that case the vortices are immersed in the variable strain generated by the rest of the flow field, it will be seen that the timescale of the variation is long compared to the turnover times of the cores, and that the asymptotic theory is therefore applicable.

It is clear that the two- and three-dimensional results are related, since Lundgren (1982) provided a general transformation that associates a strictly two-dimensional flow to any quasi-two-dimensional strained one, defined as independent of the direction $z$ except for an applied strain $\gamma$ parallel to the $z$-axis.

Consider a solution of the three-dimensional Navier–Stokes equations, formed by the superposition of a two-component velocity $\boldsymbol{u}^* = (u^*, v^*, 0)$ depending only on

$(x^*, y^*, t^*)$, and of a triaxial strain $(\alpha x^*, \beta y^*, \gamma z^*)$. The three principal strains satisfy $\alpha + \beta + \gamma = 0$, and $\gamma$ is assumed to be positive. The vorticity $\omega^*(x^*, y^*, t^*)$ is parallel to the $z$-axis.

Lundgren's transformation states that there is a related two-dimensional flow in which the axial strain $\gamma$ is absent, defined by

$$\boldsymbol{u} = (\gamma t)^{-1/2}(u^*, v^*) + s(\gamma t)^{-1}(x, -y), \qquad \boldsymbol{\omega} = (\gamma t)^{-1}\omega^*, \qquad s = (\alpha - \beta)/2\gamma t, \tag{1.1}$$

where the coordinates and time are transformed by

$$x = x^*(\gamma t)^{-1/2}, \quad y = y^*(\gamma t)^{-1/2}, \quad \gamma t = \exp(\gamma t^*). \tag{1.2}$$

In essence, the two flows behave similarly, but the velocities and the vorticities of the strained flow are amplified, its distances contract, and its time, which is proportional to the eddy turnover period, runs faster.

In the case of a Burgers' vortex, in which $\alpha = \beta = -\gamma/2$ and the three-dimensional solution is

$$\omega^* = \omega_0^* \exp(-\gamma r^{*2}/4\nu), \tag{1.3}$$

the transformed two-dimensional flow is the viscous spreading vortex

$$\omega = (\omega_0^*/\gamma t)\exp(-r^2/4\nu t). \tag{1.4}$$

For triaxially strained vortices, the correspondence with two-dimensional vortices in a plane strain is not complete, since it follows from (1.1) that the two-dimensional strain should decrease in inverse proportion to time. The reason becomes clear once the governing dimensionless parameters are considered. It is found in MKO94 that the relevant perturbation parameter for the strained vortex is, to lowest order, $\epsilon_1 = (\nu/\Gamma)(\beta - \alpha)/\gamma$, which is proportional to $(\beta - \alpha)/\omega_0^*$. The triaxial strain $(\alpha, \beta, \gamma)$ can be understood as the superposition of an axisymmetric stretching $(-\gamma/2, -\gamma/2, \gamma)$, which can be eliminated using Lundgren's formula, and a plane equatorial component $(\alpha - \beta, \beta - \alpha, 0)/2$. The perturbation parameter is the ratio of this equatorial strain to the characteristic vorticity of the vortex core.

This is the same parameter identified by Ting & Tung (1965) for the two-dimensional diffusing vortex but, in that case, as the vortex diffuses and its core vorticity decays, the driving strain has to decrease continuously if similarity is to be maintained. Alternatively, if the vortex diffuses in a constant straining flow, it suffers an increasing deformation as it spreads and becomes weaker.

Because the internal timescale of the vortex core is much faster than the viscous time, the spreading vortex can be treated as quasi-steady, and corresponds to the triaxial case to lowest order, but the difference appears at higher orders. It is found in MKO94 that, for orders beyond $O(\epsilon_1^2)$, the two factors $\gamma/\omega_0^*$ and $(\beta - \alpha)/\gamma$ enter independently in the solution, instead of as the single product $\epsilon_1$.

The asymptotic analysis of the structure of a two-dimensional vortex in a weak strain is developed in the next two sections. The expansion within the vortex core follows closely that for the triaxial case in MKO94, and will be discussed in the context of that paper. It is recast, however, in a slightly different form, to eliminate an apparent inconsistency in the ordering of the different perturbation terms in the far field of the vortex, and the reason for that inconsistency is discussed. The predictions of the model are then compared to the results of the turbulence simulation.

## 2. The asymptotic formulation

Consider a two-dimensional vortex of circulation $\Gamma$, subject to a straining velocity $s(x, -y)$. The velocity of the vortex and of the strain are comparable at a distance of order $R_s = (\Gamma/s)^{1/2}$, while the vortex radius spreads, over characteristic times $O(s^{-1})$, to be of order $R_v = (\nu/s)^{1/2}$. Its characteristic vorticity is then $\omega_c = \Gamma/R_v^2$. We are interested in the weakly perturbed limit in which

$$\epsilon = \frac{\nu}{\Gamma} = \frac{s}{\omega_c} = \left(\frac{R_v}{R_s}\right)^2 \ll 1. \tag{2.1}$$

If we normalize length with $R_s$ and time with $s^{-1}$, the vorticity equation becomes

$$\frac{\partial \omega}{\partial t} - \frac{\partial(\psi, \omega)}{\partial(x, y)} = \epsilon \nabla^2 \omega, \qquad \nabla^2 \psi = -\omega, \tag{2.2}$$

where the velocities are related to the stream function by $u = \partial\psi/\partial y$, $v = -\partial\psi/\partial x$, and $\psi \sim xy$ at infinity. The vortex has unit circulation and spreads only slowly, over $t = O(\epsilon^{-1/2})$, under the action of viscosity. For shorter times, its radius is small, and it looks like a point at the scale of $R_s$. The streamlines of such a point vortex flow are plotted in figure 1, where the vortex rotates counterclockwise, and the straining velocity is outgoing along the $x$-axis. The 'cat's eye' is aligned at 45° to the strain axes, and the streamlines are circular near the vortex and become more elliptical as they move away from it. Since the vortex radius is only $O(\epsilon^{1/2})$ (see equation (2.1)), its vorticity is almost totally confined well inside the dividing streamline, and is only bled slowly along the outgoing direction of the forcing strain. The situation is exactly equivalent to that in MKO94, where very long-lived vortices were found to exist in the case of a triaxial strain, even when one of the equatorial eigenvalues was extensional.

Two-dimensional strained vortices have been studied often. The stability of elliptical uniform-vorticity patches was analysed by Moore & Saffman (1971), who concluded that the strain would tear the core if, in our notation, $\epsilon > 0.15$. The stability analysis was extended to unsteady strains by Dritschel (1990), resulting in a broader class of behaviour. The full initial value problem for elliptical patches was studied by Kida (1981), and generalized to the case of vortices constructed from an arbitrary number of nested elliptical patches by Legras & Dritschel (1991) and Dritschel & Legras (1991). The same authors studied numerically the interaction of an external shear with a non-uniform vortex, and concluded that the weak vorticity at the edge of the vortex is stripped away, to the level at which $\omega/s \approx 0.11$), while the core itself remains coherent (Legras & Dritschel 1993). All these results support the idea that the vortex breaks down only when its vorticity becomes substantial in the neighbourhood of the dividing streamline in figure 1, and are consistent with the vortex being stable for $\epsilon \ll 1$.

In the units of (2.2) the core vorticity is $O(1/\epsilon)$. If inner variables were defined in which both the vorticity and the vortex radius are $O(1)$, equation (6) would remain unchanged. The corresponding timescale is the fast eddy-turnover time of the vortex core. We will be interested in solutions in which the structure of the vortex does not change on that timescale, although it may do so on the slower one of the external flow. We therefore choose inner variables,

$$(\hat{x}, \hat{y}) = \epsilon^{-1/2}(x, y), \qquad \hat{t} = t, \qquad \hat{\psi} = \psi, \tag{2.3}$$

in which the equations of motion become

$$[\hat{\psi}, \hat{\omega}] = \epsilon \mathrm{L}\hat{\omega}, \qquad \hat{\nabla}^2 \hat{\psi} = -\hat{\omega}, \tag{2.4}$$

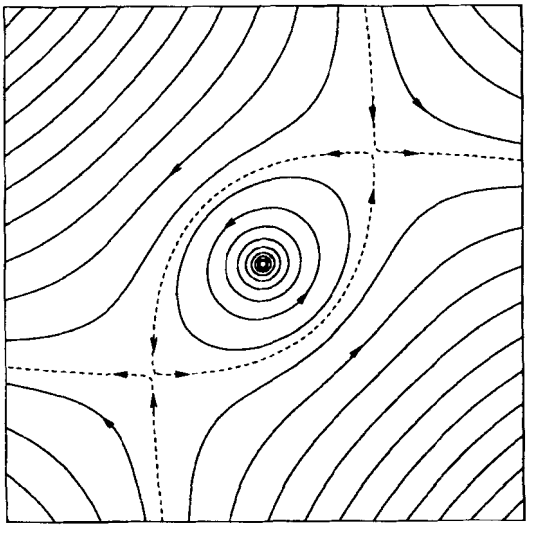

FIGURE 1. Streamlines of a point vortex in a pure strain whose principal axes are aligned to the coordinate axes.

where $[\hat{\psi}, \hat{\omega}] = \partial(\hat{\psi}, \hat{\omega})/\partial(\hat{x}, \hat{y})$ is the Jacobian, and $\mathrm{L} = \partial_{\hat{t}} - \hat{\nabla}^2$. The circulation of the vortex is still unity, but $\hat{\psi} \sim \epsilon \hat{x}\hat{y}$ at large distances. This equation is equivalent to equation (2.7) of MKO94, with the time derivative of the right-hand side substituting for the stretching operator of the three-dimensional case, as in Lundgren's transformation. We have chosen to keep the straining motion inside the definition of $\hat{\psi}$, whereas in MKO94 it was made explicit in the right-hand side. This will make the structure of the perturbation somewhat clearer.

We recall the analysis in MKO94. It is immediately obvious from (2.4) that, to the lowest approximation in $\epsilon$,

$$[\hat{\psi}_0, \hat{\omega}_0] = 0, \qquad \hat{\omega}_0 = \hat{\omega}_0(\hat{\psi}_0), \tag{2.5}$$

where we are assuming an expansion $\hat{\omega} = \hat{\omega}_0 + \epsilon\hat{\omega}_1 + \ldots$, and a similar one for $\hat{\psi}$. We will only consider cases in which this lowest-order motion is axisymmetric, $\hat{\psi}_0(\hat{r})$, in polar coordinates $(\hat{r}, \theta)$ centred on the vortex.

The first-order perturbation is

$$[\hat{\psi}_0, \hat{\omega}_1] + [\hat{\psi}_1, \hat{\omega}_0] = \frac{1}{\hat{r}}\frac{\partial}{\partial\theta}\left(\hat{\omega}_1\frac{\partial\hat{\psi}_0}{\partial\hat{r}} - \hat{\psi}_1\frac{\partial\hat{\omega}_0}{\partial\hat{r}}\right) = \mathrm{L}\hat{\omega}_0. \tag{2.6}$$

Averaging over $\theta$, we arrive at the compatibility condition

$$\mathrm{L}\hat{\omega}_0 = \frac{\partial\hat{\omega}_0}{\partial\hat{t}} - \hat{\nabla}^2\hat{\omega}_0 = 0, \tag{2.7}$$

whose solution corresponding to a point vortex at $t = 0$ is

$$\hat{\omega}_0 = \frac{1}{4\pi t}\,\mathrm{e}^{-\hat{r}^2/4\hat{t}}. \tag{2.8}$$

Substituting (2.7) into (2.6) we also get

$$[\hat{\psi}_0, \hat{\omega}_1] + [\hat{\psi}_1, \hat{\omega}_0] = 0, \tag{2.9}$$

a linear homogeneous equation which is however forced by the boundary condition

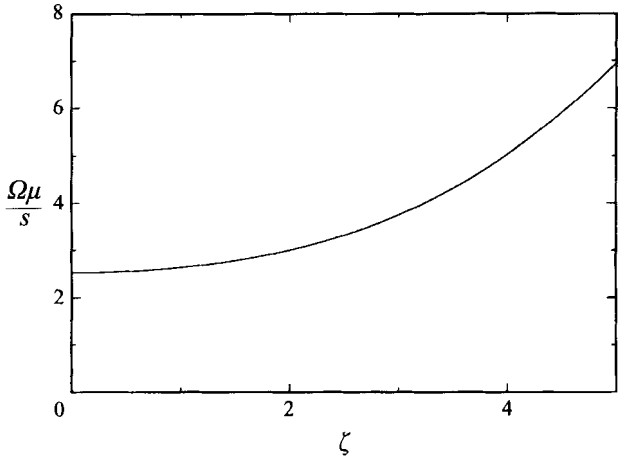


FIGURE 2. Normalized ellipticity of streamlines in the vortex core. The 1/e vorticity level is at $\zeta = 2$.

for $\hat{\psi}_1$ at infinity. It can be solved to give

$$\hat{\psi}_1 = 2t\left(\frac{\zeta^2}{4} - f(\zeta)\right)\sin 2\theta, \quad \zeta = \hat{r}/\hat{t}^{1/2}, \tag{2.10}$$

where the function $f$, as given in MKO94, satisfies

$$f'' + \frac{1}{\zeta}f' - \frac{4}{\zeta^2}f + \left(\frac{\zeta^2}{4} - f\right)\frac{\zeta^2}{4(\mathrm{e}^{\zeta^2/4} - 1)} = 0, \tag{2.11}$$

and the boundary conditions $f = O(\zeta^2)$ for $\zeta \to 0$, and $f = O(\zeta^{-2})$ for $\zeta \to \infty$. A possible axisymmetric component vanishes because of the compatibility condition at $O(\epsilon^2)$.

The resulting streamlines are elliptical, with their major axes aligned at 45° to the strain, in line with the axis of the cat's-eye pattern in figure 1, and with an ellipticity which does not vanish at the origin. If we denote the major and minor semi-axes as $a$ and $b$, the ellipticity is

$$\mu = \frac{a-b}{a+b} = \epsilon\frac{|\hat{\psi}_1|_{max}}{\hat{r}|\hat{\psi}_{0\hat{r}}|} + O(\epsilon^2) = \frac{s}{\Omega}\frac{\zeta^2/4 - f(\zeta)}{1 - \mathrm{e}^{-\zeta^2/4}} + O(\epsilon^2), \tag{2.12}$$

where $\Omega$ is the (dimensional) maximum vorticity at the centre of the vortex. The quantity $\mu\Omega/s$ is plotted in figure 2. It tends to 2.5259... at the origin, and increases for large radii, to merge into the inner streamlines of figure 1.

## 3. The far field

The procedure outlined in the previous section is the one followed in MKO94, and results in an expression for the perturbed vorticity which behaves at large radii as $\hat{\omega} \sim \exp(-\hat{r}^2/4t)(1 + O(\epsilon\hat{r}^4) + O(\epsilon^2\hat{r}^8) + \ldots)$, and which becomes inconsistent when $\hat{r} = O(\epsilon^{-1/4})$. Since this is a narrower range than the characteristic size of the cat's-eye, $\hat{r} = O(\epsilon^{-1/2})$, it raises some concern about the uniform validity of the perturbation scheme (MKO94). In particular, the asymptotic series inside the parentheses has the same ordering of terms as $\exp(\epsilon\hat{r}^4)$, which could dominate the exponent at long distances, and compromise the exponential decay of the vorticity. What is needed

is an intermediate asymptotic procedure for the construction of an exponentially decaying vorticity in the full range of radii $1 \ll \hat{r} \ll \epsilon^{-1/2}$, and which can be matched to the inner expansion given above. We discuss now how such a solution can be constructed.

An alternative way of interpreting (2.5) and (2.9) is that

$$[\hat{\psi}_0 + \epsilon\,\hat{\psi}_1,\ \hat{\omega}_0 + \epsilon\,\hat{\omega}_1] = O(\epsilon^2), \tag{3.1}$$

so that $\hat{\omega} = \hat{\omega}(\hat{\psi})$ to that order. The perturbed streamlines were compared to the isovorticity lines in MKO94, and did not agree with each other. However, the streamlines considered there corresponded only to the rotational part associated with the vortex, and did not include the forcing contribution of the strain. In the present two-dimensional situation, once the forcing is included, it is easy to show that (3.1) is satisfied.

In fact, equation (2.9) can be written, after $\theta$-integration, as

$$\hat{\omega}_1 = \hat{\omega}_{0r}\,\hat{\psi}_1/\hat{\psi}_{0r}, \tag{3.2}$$

so that the perturbed vorticity can be expressed as

$$\hat{\omega} = \hat{\omega}_0 + \epsilon\,\hat{\omega}_1 = \hat{\omega}_0(R) + O(\epsilon^2), \qquad R = \hat{r} + \epsilon\,\hat{\psi}_1/\hat{\psi}_{0\hat{r}}. \tag{3.3}$$

The expansion has been transferred from $\hat{\omega}$ to the deformed independent variable $R$. At large radii the forcing strain dominates, and $\hat{\psi}_1 \sim \hat{r}^2 \sin 2\theta$, while $\hat{\psi}_{0\hat{r}} \sim 1/\hat{r}$, which is the contribution from the central vortex. Therefore $R = \hat{r} + O(\epsilon\,\hat{r}^3)$, and the expansion of $R$ remains valid out to $\hat{r} = O(\epsilon^{-1/2})$, i.e. $r = O(1)$.

This *ad-hoc* procedure becomes cumbersome at higher orders, but a more systematic one can be implemented in the far field, outside the vortex core. The assumption is that the core remains compact and that the vorticity decays exponentially for $\hat{r} \gg 1$, so that the flow becomes irrotational. There then exists a complex potential that can be expanded in a Laurent series around the origin, and whose coefficients can be determined by matching to the inner solution where $\hat{r} = O(1)$. In this outer region the Poisson equation in (2.4) is not needed, and the problem becomes a linear diffusion–advection equation for the exponentially weak vorticity.

The form of the vorticity expansion in MKO94, where the $2n\theta$ Fourier component was found to be $O(\epsilon^n)$, suggests that the streamfunction at large distances should have the form

$$\hat{\psi} = -\frac{1}{2\pi}\log\hat{r} + \epsilon(\hat{r}^2/2 + A_2\hat{r}^{-2})\sin 2\theta + \epsilon^2(A_4\sin 4\theta + B_4\cos 4\theta)\hat{r}^{-4} + \ldots \tag{3.4}$$

where

$$A_n = \frac{\epsilon^{-n/2}}{2\pi n}\int\int \hat{\omega}(\hat{r},\,\theta)\hat{r}^{n+1}\sin n\theta\,\mathrm{d}\hat{r}\,\mathrm{d}\theta, \quad B_n = \frac{\epsilon^{-n/2}}{2\pi n}\int\int \hat{\omega}(\hat{r},\,\theta)\hat{r}^{n+1}\cos n\theta\,\mathrm{d}\hat{r}\,\mathrm{d}\theta \tag{3.5}$$

can be computed from the inner expansion.

Let us now introduce a deformed radial coordinate

$$\hat{r} = R + \epsilon R_1(R, \theta, t) + \ldots \tag{3.6}$$

and require that $\hat{\omega}$ be only a function of $R$ and $t$, and that its asymptotic expansion be uniformly valid out to $R = O(\epsilon^{-1/2})$. The streamfunction can be expressed as a function $\hat{\psi}(R, \theta, t)$, and the first equation in (2.4) becomes

$$\frac{\partial}{\partial\theta}(\hat{\psi}\,\hat{\omega}_R) + \epsilon\hat{r}\hat{r}_R\,\mathrm{L}\hat{\omega} = 0, \tag{3.7}$$

where the partial derivatives assume that everything is expressed in terms of $(R, \theta)$, and where the operator L also has to be expressed in terms of the new variables. Because the Laplacian in L is a second-order operator, and because the change to new variables is given only implicitly by (3.6), this step involves some algebraic complication, but it is easily programmed in a symbolic manipulator. The results given below were obtained using Maple. We define the expansions

$$\hat{\psi}\,\hat{\omega}_R = \hat{\psi}_0(R)\hat{\omega}_R + \sum_{n=1} \epsilon^n J_n, \qquad \hat{r}\hat{r}_R\,\mathrm{L}\hat{\omega} = \sum_{n=0} \epsilon^n H_n, \tag{3.8}$$

and separate $H_n$ into axisymmetric and non-axisymmetric parts:

$$H_n = \bar{H}_n + H_n^*, \qquad \bar{H}_n = \frac{1}{2\pi}\int_0^{2\pi} H_n\,\mathrm{d}\theta. \tag{3.9}$$

As in the previous section, the $\epsilon^n$ term of (3.7) separates into

$$\bar{H}_{n-1} = 0 \tag{3.10}$$

and

$$J_n + \int_0^{\theta} H_{n-1}^*\,\mathrm{d}\theta = \text{funct.}(R, t), \tag{3.11}$$

where the right-hand side of (3.11) is a free integration 'constant', and $J_n$ comes from the series expansion of $\hat{\psi}(r, \theta)$ in terms of the new variables. It takes the form

$$J_n = (\hat{\psi}_{0R}R_n + \hat{\psi}_n)\,\hat{\omega}_{0R} + \ldots, \tag{3.12}$$

where the extra terms involve only $R_i$ for $i < n$. That is also true of $H_{n-1}$, and (3.11) can therefore be used to determine $R_n$ as

$$R_n = \tilde{R}_n(R, \theta, t) + Q_n(R, t), \tag{3.13}$$

with the arbitrary integration function $Q_n$. The axisymmetric part (3.10) has the form

$$R^{-1}\bar{H}_n = \mathrm{L}_0\,\hat{\omega}_n = \text{r.h.s.}(Q_n, \ldots), \tag{3.14}$$

where $\mathrm{L}_0 = \partial_t - \nabla_R^2$, and $\nabla_R^2$ is the Laplacian operator in the variables $(R, \theta)$ although, as it is always applied to the functions $\hat{\omega}_n(R, t)$, only its radial part is of interest. At this stage the function $Q_n$ can be chosen to control the growth of $\hat{\omega}_n$ with $n$ at large $R$.

We will now indicate the structure of the first few orders of the expansion, and the results for the particular case of the streamfunction (3.4). The $O(1)$ equations are identical to those in the previous section. Our choice of $R_0 = R$ makes $J_0$ identically zero, and the first axisymmetric equation is

$$R^{-1}\bar{H}_0 = \mathrm{L}_0\hat{\omega}_0 = 0, \qquad \hat{\omega}_0 = \frac{1}{4\pi t}\,\mathrm{e}^{-R^2/4t}. \tag{3.15}$$

There is no angular component at this order, and the non-axisymmetric equation at $O(\epsilon)$ is

$$J_{1\theta} = \frac{\partial}{\partial\theta}(\hat{\psi}_{0R}R_1 + \hat{\psi}_1) = 0, \qquad R_1 = -\hat{\psi}_1/\hat{\psi}_{0R} + Q_1(R, t). \tag{3.16}$$

For the streamfunction (3.4),

$$R_1 = \pi(R^3 + 2A_2/R)\sin 2\theta + Q_1(R, t). \tag{3.17}$$

The rest of the equation at this order is

$$\mathrm{L}_0\hat{\omega}_1 = f(R_1, \hat{\omega}_0), \tag{3.18}$$

where the right-hand side is a linear and homogeneous functional of $R_1$. Since the angular average of $\hat{\psi}_1$ vanishes, it follows from (3.16) that the average of $R_1$ is the arbitrary additive function $Q_1$, and that the right-hand side of the axisymmetric component of (3.16) is homogeneous in $Q_1$. We can therefore choose $Q_1 = \hat{\omega}_1 = 0$.

The first order for which this is not possible is $O(\epsilon^2)$. The non-axisymmetric part of the equation needs no special treatment. For the particular case (3.4) the leading terms are

$$R_2 = -(\hat{\psi}_{1R}R_1 + \hat{\psi}_{0RR}R_1^2/2)/\hat{\psi}_{0R} + \ldots = Q_2 + \pi^2 R^5\left((3/t)\cos 2\theta - \tfrac{5}{4}\cos 4\theta\right) + O(R^3). \tag{3.19}$$

In the axisymmetric equation, however, the right-hand side contains quadratic terms in $R_1$ which have non-zero angular average, and the equation for $\hat{\omega}_2$ is no longer homogeneous. For our special case we obtain

$$\mathrm{L}_0\hat{\omega}_2 = \frac{\mathrm{e}^{-R^2/4t}}{32\pi t^3}\left(7\pi^2 R^6 - 4R^2 Q_{2R} + O(R^4)\right). \tag{3.20}$$

The solution of (3.18) would result in $\hat{\omega}_2 \sim R^6\exp(-R^2/4t)$, and would limit the convergence of the expansion to $\hat{r} = O(\epsilon^{-1/3})$. We can now use $Q_2$ to cancel as many of the high powers of $R$ in the right-hand side of the equation as needed, so that the leading term of the solution is at most proportional to $R^4\exp(-R^2/4t)$, and the expansion remains valid to the desired distance. In the present case it is enough to take

$$Q_2 = 7\pi^2 R^5/20. \tag{3.21}$$

Note that $R_n/R \sim R^{2n}$ at large distances, guaranteeing a uniform ordering of the terms of the coordinate deformation out to $\hat{r} = O(\epsilon^{-1/2})$. The convergence of the series for $\hat{\omega}$ has already been discussed.

It is also clear how our result can be matched to the inner expansion of MKO94. We can invert our expression for $\hat{r}$ to give

$$R = \hat{r} - \epsilon\hat{r}^3\pi\sin 2\theta + \ldots, \tag{3.22}$$

and expand the leading term of our series

$$\hat{\omega} = \frac{1}{4\pi t}\mathrm{e}^{-R^2/4t} + O(\epsilon^2) \approx \frac{1}{4\pi t}\mathrm{e}^{-\hat{r}^2/4t}(1 + \epsilon\pi\hat{r}^4 t^{-1}\sin 2\theta + \ldots), \tag{3.23}$$

which is equivalent to the expansion in MKO94 for $\hat{r} \gg 1$.

The success of the coordinate deformation in controlling the non-uniformities of the expansion is not surprising. The perturbation scheme used here and in MKO94 is a variant of the averaging method which has been known in different forms at least since the work of Lagrange in the eighteenth century. It was first developed for Hamiltonian perturbations, and this application is reviewed by Arnold (1978). It was soon understood that the use of appropriate coordinates was important for the success of the scheme, which depends on the approximate correspondence of different types of averaging. It is of interest to note that the left-hand side of (2.4) has a Hamiltonian form, with either the streamfunction or the vorticity acting as Hamiltonians. Its right-hand side does not preserve that structure and the use of strict Hamiltonian techniques, although indicative, is not necessary. The use of coordinate deformations in more general applications is discussed by Van Dyke (1975). The *a*

*posteriori* scheme that led to (3.3) is identified there as due to Pritulo (1962), while the more general scheme used later is associated with Poincaré. There is, in principle, no reason why the latter scheme could not be used to obtain a uniformly valid expansion at all distances within the cat's-eye, but the nonlinearity associated with the coupling of the streamfunction to the vorticity makes the algebra unwieldy at the higher orders inside the vortex core. The approach used here is sufficient to display the physical character of the solution, while keeping algebraic complication to a minimum. A somewhat similar approach, applied to uniform vortex patches and using conformal deformations to regularize the expansion, was used by Jiménez (1988).

## 4. Numerical experiments

The predictions in the previous sections are checked next against the structure of vortices in a numerical simulation of decaying two-dimensional turbulence in a periodic square domain at high Reynolds number. The code is a standard spectral Fourier approximation to the vorticity equation, fully de-aliased, with a third-order Runga–Kutta method for time advancement. It uses Newtonian viscosity, and the Reynolds number, based on the side of the domain $L$ and on the initial root-mean-square fluctuation velocity $u'$, is $5.5 \times 10^4$.

The numerical resolution is $1024^2$ Fourier modes before de-aliasing, corresponding to a maximum numerical wavenumber $k_{max} = 341$. The initial conditions are chosen with a random phase, and with an energy spectrum decaying slowly (like $k^{-3/2}$) for $k \leqslant 200$, and much faster ($k^{-7}$) for higher wavenumbers. After $u't/L \approx 0.2$, the vorticity concentrates into compact vortices (McWilliams 1984) scattered over a much weaker background. The results used here are compiled at $u't/L \approx 1.65$–$1.85$. By that time the total enstrophy has decayed by a factor of 400 from the initial condition, while the energy has only decayed by 40%, and there are approximately 100 identifiable vortices in the computational box.

The mean radius of the vortices is $\bar{r} = 0.015L$, which agrees in order of magnitude with the radius of a viscous vortex spreading from an initial point, $r_v = 2(\nu t)^{1/2} \approx 0.01L$. It should be compared to the larger average separation between vortices, $D \approx 0.1L$. The mean Reynolds number of individual vortices is $\bar{\Gamma}/\nu \approx 3500$. The timescale for the evolution of the vortex distribution is $D/u'$, shorter than the turnover time, $L/u'$, but still longer than the rotation time of individual vortices, $\omega_c^{-1} = \bar{r}^2/\bar{\Gamma} \approx 5 \times 10^{-3} L/u'$. Therefore the scale separation assumed in the previous sections applies, and the results of the analysis should hold.

A catalogue of vortices is compiled at regular intervals from the computed flows fields. Candidates are identified as connected regions in which the topological discriminant (Weiss 1991)

$$Q = s^2 - \omega^2/4 \tag{4.1}$$

is more negative than a given threshold, which is chosen as a small multiple of the standard deviation of $Q$ over the whole field ($Q_t/Q' = 2.5$). The influence of this threshold was checked, and found to be small, although a good choice is important in minimizing the work involved in the subsequent filtering of the results. Each vortex candidate is characterized by its circulation, its area, its centre of gravity, and the tensor of inertia of its vorticity distribution $\int\int \omega(x_i - \bar{x}_i)(x_j - \bar{x}_j)\,\mathrm{d}S$. This tensor is used to compute the two principal moments of inertia and the orientation of the principal axes.

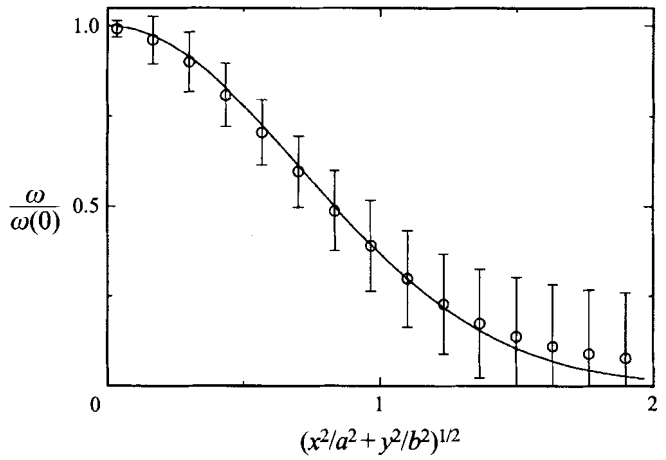


FIGURE 3. Averaged distribution of vorticity for all the vortices of the numerical catalogue, with respect to their radial elliptical coordinate. Solid line is equation (4.2).

Each vortex is assumed to have a Gaussian vorticity distribution in elliptical coordinates aligned with those axes,

$$\omega_M = \Omega \exp(-x'^2/a^2 - y'^2/b^2), \qquad a \geqslant b. \tag{4.2}$$

The three parameters, $a$, $b$, $\Omega$, and the dimensionless 'radius' $\rho$ of the original patch, are obtained by equating the measured values for the area, the circulation, and the principal moments to those of an elliptical vortex of the form (4.2), contained inside $x'^2/a^2 + y'^2/b^2 < \rho^2$. The result is a set of positions, areas $S = \pi ab$, circulations $\Gamma = S\Omega$, and orientations of the major axes $\phi_\omega$. Candidates with no solution for the model parameters, and those originating from patches formed by less than four grid points, are eliminated at this stage.

The assumption (4.2) for the vorticity distribution is tested next. Assuming an elliptical Gaussian vortex, it is easy to show that the contour for which $Q = 0$ should correspond to $\rho \approx 1$ and, in consequence, only vortices with $0.5 < \rho < 1.5$ are kept in the database. The fit between the model (4.2) and the actual flow vorticity is also tested directly. The mean-square deviation $\epsilon_\omega^2 = \overline{(\omega - \omega_M)^2}$ is computed over all the points of the original patch, and candidates for which $\epsilon_\omega/\Omega > 0.2$ are discarded. This procedure was found to work reasonably well in identifying vortices, while missing only a few percent of those which could be identified visually, usually very deformed ones involved in close interactions. The total enstrophy contained in our vortex catalogue is about 70% of the total, concentrated in 5% of the total area. A comparison of the Gaussian model with the mean and standard deviations of the measured vorticities is given in figure 3. Note that only points inside the original patch, for which $Q \leqslant Q_t \approx 0$, are used in the computation of $\epsilon_\omega$, and that the Gaussian fit outside $x'^2/a^2 + y'^2/b^2 \approx 1$ is not guaranteed by the mean-square deviation test. The total sample includes about $10^4$ vortices over 160 different flow fields, corresponding to about 100 different vortex histories. Only 70% of them have ellipticities that are high enough ($a/b > 1.1$) for the orientation of the major axes to be reliably defined, and those are the only ones used in our statistics. A roughly similar procedure for generating a vortex catalogue was presented by McWilliams (1990) but no data were given in that case for the enstrophy and area fractions which can be compared to the present ones.

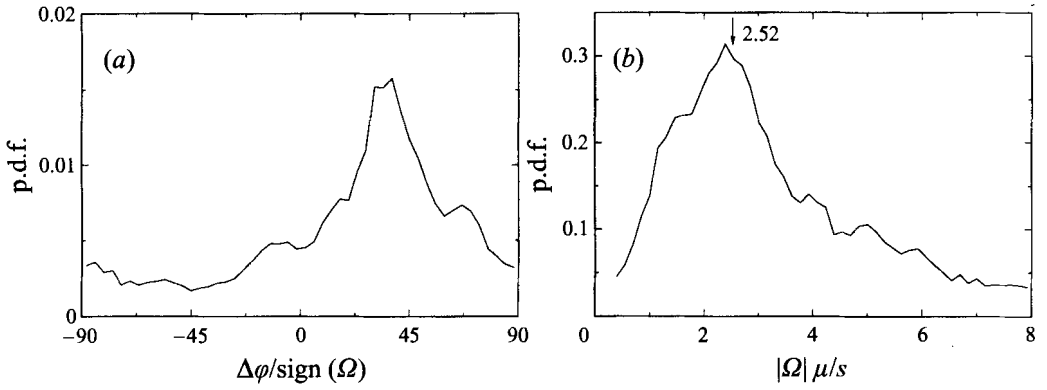


FIGURE 4. Probability density functions for the offset angle between the major axes of the vortex with respect to the extensional axes of the ambient strain, and for the reduced ellipticity of the cores, defined as in figure 2.

The next step is to determine an 'ambient' strain $s$ at the position of each vortex. Several methods were tried, and the one selected was to use the strain generated at the centre of gravity of each vortex by all the other vortices in the database. The result changes only slightly if the other vortices are treated as points or as full Gaussian models, with the correlation coefficient between the results of both methods being over 0.95. In contrast, the simple method of subtracting the Gaussian model for the vortex in question and computing the strain generated by the rest of the flow proved to be inadequate. A typical value for the ratio $s/\Omega$ is 0.05, and the small vorticity residuals left by the difference between the actual and the modelled vorticity distributions are enough to mask the ambient strain generated by the rest of the flow. For each vortex a strain magnitude and an orientation $\phi_s$ of the extensional axis are generated in this manner.

These data allow us to check the results obtained in §2 for the orientation and ellipticity of the vorticity distribution with respect to the driving strain. In particular, the axes of the vortices should be offset with respect to those of the strain by 45° in the sense of rotation of the vortex, and their ellipticity, defined as in (2.12), should be close to $2.52s/\Omega$. Both conclusions are tested in figure 4. Although there is considerable statistical scatter, it is clear that the maxima of both histograms agree well with the theoretical analysis.

The assumptions on the timescales of the flow can also be now checked directly. A measure of the rate of change of the imposed strain is $\sigma = |\mathrm{d}s_{11}/\mathrm{d}t|/|s|$, where $s_{11}$ is one of the components of the imposed strain tensor. From the vortex catalogue $\sigma \approx 2|s|$ on the average, so that the evolution time of the strain is of the same order as the straining time itself. They are both, however, longer than the rotation time, and $\sigma/s \approx 0.1$.

During the review process of this paper one of the referees remarked that the steady strain used in this paper is only a particular case of the general one in which the strain rotates and varies with time, and that a more realistic model for the deformations in two dimensions would include an additional solid-body rotation component of $O(s)$. The results in the previous paragraph lend strength to that remark, and pose the question of the reason for the agreement in figure 4.

It is however easy to see that the addition of an axisymmetric component to the perturbation streamfunction does not change the results of the analysis in §§2–3.

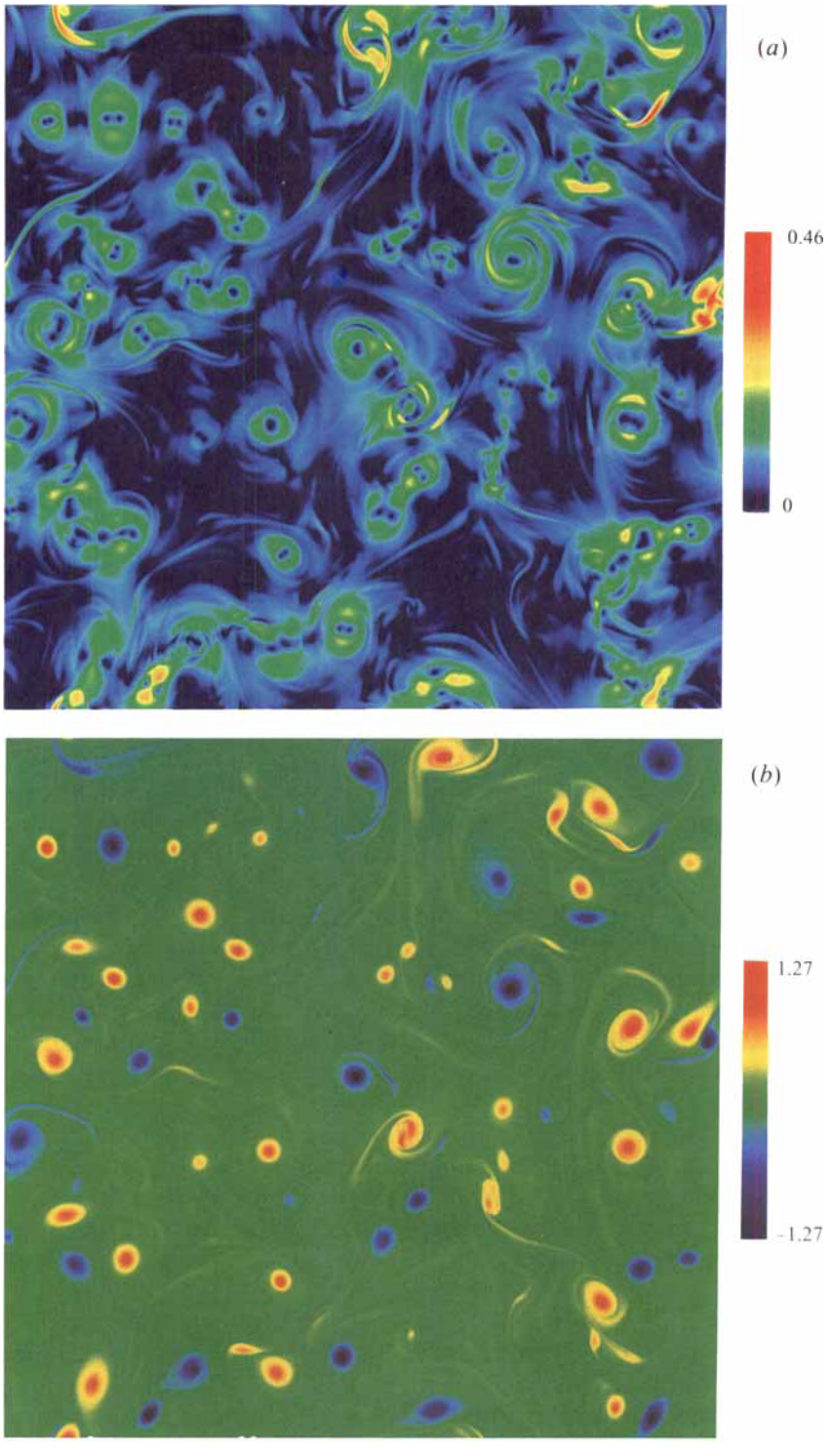


FIGURE 5. Typical total strain (*a*) and vorticity (*b*) fields for the two-dimensional turbulent flow used in the text.

Because (2.6) and (2.9) are insensitive to components of $\hat{\psi}_1$ which are only functions of $\zeta$, the equation satisfied by $f(\zeta)$ is not changed, and the shape of the vorticity distribution is not modified to $O(\epsilon)$. To this order the vortex follows the imposed strain even if the latter rotates on a timescale comparable to its own deformation time. In essence, while the effect of the strain is visible to first order because the lowest-order axisymmetric vortex generates no radial velocities which could compete with it, the effect of a comparable rotation appears only at $O(\epsilon^2)$ because it competes directly with the much stronger azimuthal velocity of the vortex.

We have dealt up to now with the ambient strain which would be present at the location of the vortex if the vortex were not present. One of the striking results in MKO94 was the structure of the *total* strain (or equivalently dissipation) produced by the driving flow and by the vortex itself. In a circular core the total strain is zero at infinity and at the centre of the core, and is maximum in an annulus at the periphery of the vortex. When the axisymmetry is broken by the driving strain, the crown of maxima is deformed into two crescents aligned with the major axis of the vortex ellipse, while the central minimum splits into two minima aligned to the minor axis (see figure 7 of MKO94). The same structure can be seen many times in the map of total strain for a typical turbulent field in figure 5(*a*). A comparison with the vorticity map in figure 5(*b*) confirms that the strain structures do indeed correspond to the elliptical vortices.

## 5. Discussion

In the first part of this paper we have given an asymptotic expansion for the structure of a two-dimensional viscous vortex in a weak plane strain. The results are similar to those of Ting & Tung (1965) and in MKO94, but the expansion is extended up to distances $\hat{r} = O(\epsilon^{-1/2})$, which is the scale of the cat's-eye streamline separating the elliptic points dominated by the effect of the vortex from the hyperbolic region dominated by the driving strain. In the limit studied here, $Re_\Gamma \gg 1$, the radius of the core itself is much smaller, and it behaves like a point vortex with respect to the external flow. The non-uniformity mentioned above refers to distances much greater than the core radius but smaller than the cat's-eye, and was present in the expansions in both of the papers cited, although it was only explicitly recognized in the second one. It is removed here by using a coordinate deformation in conjunction with the basic averaging technique of the previous studies.

The results confirm that the vorticity is approximately Gaussian in distorted coordinates, which coincide roughly with the flow streamlines. It is therefore exponentially small in the neighbourhood of the dividing streamline, from where it is presumably slowly stripped to infinity (MKO94).

In the present context of steady, or self-similar, solutions, the validity of the expansion cannot be extended farther from the core, since it was shown in Appendix A of MKO94 that no steady solution could be expected for the vorticity distribution in any part of the flow dominated by a strain with an extensional direction. It is only well inside the dividing streamline that the vortex shelters itself from the external influence, and that a self-similar solution is possible.

The predictions of the asymptotic expansion on the shape and orientation of the vorticity distribution are tested against a vortex catalogue obtained from a numerical simulation of two-dimensional turbulence. They are shown to agree well with the numerical experiment, and the same is true of the spatial distribution of the total strain (or dissipation) field.

It is interesting that this is so even if the vortices in two-dimensional turbulence are subject to strains which are not steady. The basic requirement for the asymptotic expansion in this paper is that the timescale of the driving flow should be much longer than the turnover period of the core, which is equivalent to $Re_\Gamma \gg 1$. This was sharpened recently by Lingevitch & Bernoff (1995) who studied the initial-value problem of a viscous vortex subject to a sudden change in the external driving flow, and showed that the relaxation time is $O(\Omega^{-1} Re_\Gamma^{1/3})$, as conjectured in MKO94, §2. In a two-dimensional turbulent field with vortices of circulations $O(\Gamma)$ and radii $O(a)$, separated by distances $O(D)$, the evolution time for the strain is $O(D^2/\Gamma)$, and the condition that it should be much longer than the relaxation time of the individual cores is that

$$D^2\Omega/\Gamma \approx D^2/a^2 \gg Re_\Gamma^{1/3}. \tag{5.1}$$

In our example this is marginally satisfied, since the left-hand side is approximately 100, while the right-hand side is of order 15, but it is not clear whether the same would be true for simulations at higher Reynolds numbers or at different times in their evolution.

This research was partially supported by the Human Capital and Mobility program of the EU under contract CHRXCT920001.

## REFERENCES

ARNOLD, V. I. 1978 *Mathematical Methods of Classical Mechanics*, §10. Springer.

DRITSCHEL, D. G. 1990 The stability of an elliptical vortex in an external straining flow. *J. Fluid Mech.* **210**, 223–261.

DRITSCHEL, D. G. & LEGRAS, B. 1991 The elliptical model of two dimensional vortex dynamics II: disturbance equations. *Phys. Fluids* A **3**, 855–869.

JIMÉNEZ, J. 1988 Linear stability of a nonsymmetric, inviscid, Kármán street of small uniform vortices. *J. Fluid Mech.* **189**, 337–348.

KIDA, S. 1981 Motion of an elliptic vortex in a uniform stream. *J. Phys. Soc. Japan* **50**, 3517–3520.

LEGRAS, B. & DRITSCHEL, D. G. 1991 The elliptical model of two dimensional vortex dynamics I: the basic state. *Phys. Fluids* A **3**, 845–854.

LEGRAS, B. & DRITSCHEL, D. G. 1993 Vortex stripping and the generation of high vorticity gradients in two dimensional flows. *Appl. Sci. Res.* **51**, 445–455.

LINGEVITCH, J. F. & BERNOFF, J. 1995 Distortion and evolution of a localised vortex in an irrotational flow. *Phys. Fluids* **7**, 1015–1026.

LUNDGREN, T. S. 1982 Strained spiral vortex model for turbulent fine structure. *Phys. Fluids* **25**, 2193–2203.

MCWILLIAMS, J. C. 1984 The emergence of isolated coherent vortices in turbulent flow. *J. Fluid Mech.* **146**, 21–43.

MCWILLIAMS, J. C. 1990 The vortices of two-dimensional turbulence. *J. Fluid Mech.* **219**, 361–385.

MOFFATT, H. K., KIDA, S. & OHKITANI, K. 1994 Stretched vortices – the sinews of turbulence; large Reynolds number asymptotics. *J. Fluid Mech.* **259**, 241–264 (referred to herein as MKO94).

MOORE, D. W. & SAFFMAN, P. G. 1971 Structure of a line vortex in an imposed strain. In *Aircraft Wake Turbulence and its Detection* (ed. J. H. Olson, A. Goldburg & M. Rogers), pp. 339–354. Plenum.

PRITULO, M. F. 1962 On the determination of uniformly accurate solutions of differential equations by the method of perturbation of coordinates. *J. Appl. Math. Mech.* **26**, 661–667.

TING, L. & TUNG, C. 1965 Motion and decay of a vortex in a nonuniform stream. *Phys. Fluids* **8**, 1039–1051.

VAN DYKE, M. 1975 *Perturbation Methods in Fluid Mechanics*, §7 and Note 3. Parabolic.

WEISS, J. 1991 The dynamics of enstrophy transfer in two-dimensional hydrodynamics. *Physica* D **48**, 273–294.